Biomedicine & Pharmacotherapy 169 (2023) 115668

Contents lists available at ScienceDirect

Biomedicine & Pharmacotherapy

journal homepage: www.elsevier.com/locate/biopha

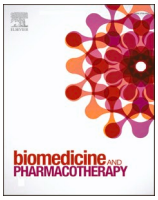

Tetrazole derivatives as potent immunomodulatory agents in tumor microenvironment

Alberto Pla-López, Miguel Carda, Eva Falomir *

Inorganic and Organic Chemistry Department, University Jaume I, E-12071 Castellón, Spain

ARTICLE INFO

Keywords:
Amine
Antiproliferative activity
Apoptosis
CD-47
C-Myc
PD-L1
Tetrazole
THP-1
TNF-α
VEGFR-2

ABSTRACT

Twenty-seven compounds bearing a tetrazole ring as a central unit have been designed, synthetized and biologically evaluated. Studies have been performed in order to compare the effect of tetrazole derivatives bearing amine electron-donor or nitro electron-acceptor groups. The antiproliferative activity has been determined in monoculture studies on tumor cell lines HT-29, A-549, MCF-7 and on non-tumor cell line HEK-293 as well as in co-culture studies (HT-29/THP-1). All the compounds have been studied as PD-L1 (Programmed Death Ligand 1), VEGFR-2 (Vascular Endothelial Growth Factor 2), CD-47 (Cluster of Differentiation 47) and c-Myc inhibitors. The effect on TNF-α secretion has also been determined. Bromoderivatives **23**, **24** and chloroderivatives **26**, **27** have demonstrated an apoptotic effect on HT-29 cancer cells. Compounds bearing an amine group have shown very promising effects as TME immunomodulatory agents.

1. Introduction

Research in cancer biology has allowed cancer and carcinogenesis to be redefined as a process that focuses not on the tumor cell but on the entire environment or ecosystem that surrounds it which has been called tumor microenvironment (TME). In this environment, tumor cells are joined by immune cells, secreted cellular factors and non-cellular components such as the extracellular matrix, all under physiological conditions determined by the pH and oxygen levels. For all these reasons, it is now believed that communication and interactions between tumor cells and other TME cells, such as immune cells, play a very important role in carcinogenesis [1–4].

Heterogeneity is a crucial feature of TME and determinant for the efficacy of cancer therapies. This heterogeneity extents to cell morphology, cell surface receptors, cell signaling, proliferation, migration, drug response, angiogenesis, immunogenicity and apoptosis induction [5]. In this sense, c-Myc is a transcription factor that regulates the expression of genes and proteins involved in all these processes and it is directly involved in the cancer aggressiveness [6].

In addition, c-Myc is also involved in crosstalk between cancer cells and the host, as activation of the host immune system against the tumor can lead to its regression through both innate and adaptive immune effectors [7]. CD-47 (Cluster of Differentiation 47) is essential for the innate immune system and CD247 or PD-L1 (Programmed Death Ligand 1) is crucial for the adaptive immune response [8]. It has been shown that c-Myc regulates the expression of the two immune checkpoint proteins CD-47 and PD-L1 on the surface of tumor cells and, although the effects on both expression levels were mild, the consequences on tumor regression were extremely pronounced [8]. It is therefore likely that c-Myc promotes tumorigenesis by, among other things, modulating immune regulatory molecules and, therefore, the downregulation of CD-47 and PD-L1 appears to be required for the induction of sustained tumor regression, angiogenesis arrest and senescence induction promoted by c-Myc inactivation [9].

Regarding PD-L1 in TME, it is interesting to remind that PD-L1 is also expressed by immune cells found within the TME, including lymphocytes, macrophages, and dendritic cells [10]. Clinical data had demonstrated that PD-L1 can also be expressed by peripheral monocytes, and tumor-infiltrating macrophages (TAMs), which originate mainly from peripheral monocytes, also showing high PD-L1 expression [11]. The presence of PD-L1 in monocytes may be of pathophysiological relevance and the mechanism of their regulation and the functional consequences is still under study, but indeed this fact supports novel opportunities for the optimization of immunotherapies and other anticancer strategies. Besides, nowadays, most clinical protocols go through assessing not only PD-L1 expression of tumor cells but, also, checking PD-L1 expression of

* Corresponding author.
E-mail address: efalomir@uji.es (E. Falomir).

https://doi.org/10.1016/j.biopha.2023.115668
Received 26 July 2023; Received in revised form 30 September 2023; Accepted 6 October 2023
Available online 15 November 2023

immune cells in the blood in order to predict therapy responses in patients undergoing checkpoint blockade therapy [11]. It has also been observed that the proportions of PD-L1 + monocytes tend to increase depending on disease progression, suggesting that PD-L1 expression on circulating monocytes may reflect the tumor burden rather than tumor biology [12].

When talking about TME supporting tumor cell viability, it is important to consider that inflammation is very often developed in the tumor zone through increased secretion of cytokines such as TNF-α or IL-6 [13]. The latter is ubiquitous in many types of tumors and contributes to promotion of cancer cell proliferation, epithelial-mesenchymal transition (EMT) and migration [13]. On the other hand, TNF-α is a key regulator of apoptosis and angiogenesis. It is one of the key cytokines that regulates TME with pleiotropic functions that have both pro- and anti-tumor roles. There are a lot of pre-clinical and clinical cases that demonstrate that the infiltration of high doses of TNF-α in solid tumors enhance the efficacy of immunotherapies though the mechanism of this action remains under study [14]. However, it is well established that a TNF-α level, much higher than the usual physiological level in the tumor, can enhance tumor cell death by apoptosis [14].

Over the past five years, our research has focused on the discovery of small molecules with anti-angiogenic and immunomodulatory activity and more recently we have also been investigating the potential effect of these new molecules on TME [15–19]. Among the molecules we have designed are those bearing a 1,2,3-triazole core, which were designed to inhibit VEGFR-2 and PD-L1 in cancer cells (see Fig. 1) [15,19]. These compounds reduced PD-L1 level by approximately 30–40% compared to untreated cells. In addition, some of the triazole derivatives also had a moderate effect on c-Myc expression (see Fig. 1). The activities obtained for these compounds were similar to reference compounds sorafenib, a VEGFR-2 inhibitor, and BMS-8, a PD-L1 inhibitor [20,21]. In addition, docking studies carried out in our group showed that the triazole scaffold derivatives fit both VEGFR-2 and PD-L1 binding sites.

Our aim in the present work was to make some structural modifications to our previously studied molecules to improve both the effect on c-Myc and on the release of pro-inflammatory cytokines such as IL-6 and TNF-α⊡ In the last decade, new scaffolds have been selected for the generation of novel anti-inflammatory agents with better pharmacological profiles than the existing ones [22]. In this sense, tetrazoles are good candidates thanks to their broad-spectrum of biological, pharmaceutical and clinical activities such as, anticancer, antifungal and anti-inflammatory activities [23]. We, therefore, decided to replace the triazole group with a tetrazole nucleus. We also decided to check the effect of the amine group in these molecules by preparing some derivatives with a nitro group instead. Scheme 1 (see below) shows all the tetrazole derivatives we have synthesized to determine their effect on cell proliferation, on PD-L1, VEGFR-2, CD-47 and c-Myc expression in cancer cells and on the secretion of TNF-α in co-cultures of cancer and immune cells. Thus, our main objective is to generate some small molecules with potential use as TME immunomodulators.

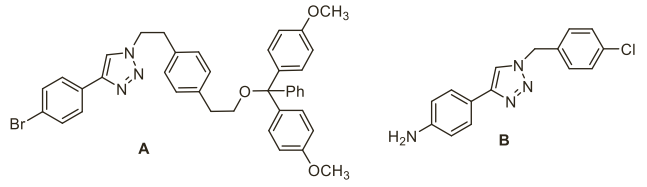

VEGFR-2, PD-L1 and c-Myc protein expressions in HT-29 cell line (%)

	VEGFR-2 (%)	PD-L1 (%)	c-Myc (%)
Sorafenib	85 ± 5	-	-
BMS-8	-	62 ± 3	99 ± 4
A	81 ± 7	47 ± 1	67 ± 8
B	69 ± 7	57 ± 17	83 ± 7

Fig. 1. Outstanding results from our molecules previously designed compared to reference compounds.

2. Experimental section

2.1. Materials and methods

2.1.1. Chemistry

2.1.1.1. General Procedures. ^{1}H and ^{13}C NMR spectra were measured at 25 °C. The signals of the deuterated solvent ($CDCl_3$ and DMSO-d_6) were taken as the reference. Multiplicity assignments of ^{13}C signals were made by means of the DEPT pulse sequence. Complete signal assignments in ^{1}H and ^{13}C NMR spectra were made with the aid of 2D homo- and heteronuclear pulse sequences (COSY, HSQC, HMBC). Infrared spectra were recorded using KBr plates. High resolution mass spectra were recorded using electrospray ionization–mass spectrometry (ESI–MS). Experiments which required an inert atmosphere were carried out under dry N_2 in oven-dried glassware. Commercially available reagents were used as received.

2.1.1.2. Synthesis of benzonitrile precursors. A solution of 1 eq. of the corresponding benzonitrile, 2 eq. of NaN_3 and 0.5 eq. of $ZnBr_2$ in *i*-PrOH:H_2O (1:2; 135 mL) was kept under stirring for 24 h at 90ºC. Then, a 10% aqueous citric acid solution (50 mL) and ethyl acetate (30 mL) were added. The aqueous phase was extracted three times with 10 mL of ethyl acetate and the collected organic phases were washed with brine. Finally, organic phase was dried over anhydrous $NaSO_4$ and the solvent was evaporated under vacuum. The residue was purified by column chromatography on silica gel using as eluent hexane:ethyl acetate (1:1; 4:6; 3:7) mixtures.

2.1.1.3. Synthesis of bromobenzyl precursors. To a solution of the corresponding benzyl alcohol (1 eq.) in CH_2Cl_2 (15 mL) was added dropwise PBr_3 (1 eq.) while keeping the flask at 0ºC. Then, the reaction mixture was kept under stirring for 2 h at room temperature. Then, the mixture was poured over a saturated aqueous $NaHCO_3$ solution and the aqueous phase was extracted three times with CH_2Cl_2 (3 ×10 mL). The collected organic phases were washed with brine and dried over anhydrous $NaSO_4$. Then the solvent was evaporated under vacuum. The residue was purified by column chromatography on silica gel using hexane:ethyl acetate (95:5) mixture.

*2.1.1.4. Synthesis and characterization of tetrazole derivatives **1**–**14**.* A NaH suspension in mineral oil (0,5 mmol, 1 eq.) was washed with pentane (3 ×1.25 mL) under inert atmosphere. After cooling at 0 ºC dry acetonitrile (3 mL) was added. After 5 min of stirring the corresponding tetrazole (0.5 mmol, 1 eq.) dissolved in the minimum quantity of acetonitrile was added. The reaction mixture was allowed to stir at room temperature for 30 min and then the corresponding benzyl halide (0.55 mmol, 1.1 eq.) and a catalytic amount of NaI were added. The reaction mixture was allowed to stir at 60 ºC for 24 h. Then, it was poured into an aqueous saturated solution of NH_4Cl (10 mL) and the aqueous phase was extracted three times with ethyl acetate (3 ×10 mL). The collected organic phases were washed with brine and dried over anhydrous $MgSO_4$. After solvent elimination under vacuum the resulting residue was purified by column chromatography on silica gel using hexane:ethyl acetate (9:1; 8:2; 7:3) mixtures.

2-Benzyl-5-phenyl-2*H*-tetrazole (1): yield = 34%; m.p. = 71–72 ºC (white solid). IR ν_{max} 3004.2, 2836.5, 1652.3, 1613.9, 1494.7, 1248.7 cm^{-1}. NMR ^{1}H (400 MHz, $CDCl_3$) δ = 8.05–8.00 (m, 2 H), 7.35–7.20 (m, 8 H), 5.65 (s, 2 H) ppm. NMR ^{13}C (100 MHz, $CDCl_3$) δ = 165.5 (C), 133.4 (C), 130.3 (CH), 129.1 (CH), 128.9 (CH), 128.8 (CH), 128.4 (CH), 127.5 (C), 126.9 (CH), 56.8 (CH_2) ppm. HR ESMS *m/z* 237.1141 $(M+H)^+$. Calculated for $C_{14}H_{12}N_4$: 237.1140.

2-Benzyl-5-(4-nitrophenyl)— 2*H*-tetrazole (2): yield = 39%; m.p.

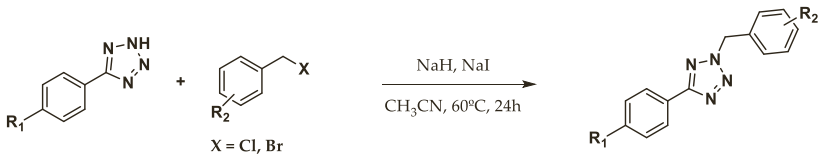

1	(34%)	R_1 = H,	R_2 = H	**8**	(32%)	R_1 = NO_2,	R_2 = *p*-OCH_3
2	(39%)	R_1 = NO_2,	R_2 = H	**9**	(23%)	R_1 = NO_2,	R_2 = *o*-Br
3	(96%)	R_1 = NO_2,	R_2 = *o*-CH_3	**10**	(39%)	R_1 = NO_2,	R_2 = *m*-Br
4	(52%)	R_1 = NO_2,	R_2 = *m*-CH_3	**11**	(17%)	R_1 = NO_2,	R_2 = *p*-Br
5	(46%)	R_1 = NO_2,	R_2 = *p*-CH_3	**12**	(12%)	R_1 = NO_2,	R_2 = *o*-Cl
6	(41%)	R_1 = NO_2,	R_2 = *o*-OCH_3	**13**	(52%)	R_1 = NO_2,	R_2 = *m*-Cl
7	(58%)	R_1 = NO_2,	R_2 = *m*-OCH_3	**14**	(59%)	R_1 = NO_2,	R_2 = *p*-Cl

Scheme 1. Synthesis of functionalized tetrazoles **1–14**.

= 143–144 ºC (yellow solid). IR ν_{max} 3004.2, 2836.5, 1652.3, 1613.9, 1523.7, 1494.7, 1248.7 cm^{-1}. NMR ^1H (300 MHz, $CDCl_3$) δ = 8.32 (s, 4 H), 7.47–7.35 (m, 5 H), 5.84 (s, 2 H) ppm. NMR ^{13}C (75 MHz, $CDCl_3$) δ = 163.7 (C), 149.0 (C), 133.4 (C), 133.0 (C), 129.4 (CH), 129.2 (CH), 128.6 (CH), 127.8 (CH), 124.3 (CH), 57.3 (CH_2) ppm. HR ESMS *m/z* 282.0991 $(M+H)^+$. Calculated for $C_{14}H_{12}N_4$: 282.0995.

2-(2-Methylbenzyl)− 5-(4-nitrophenyl)− 2*H*-tetrazole (3): yield = 96%; m.p. = 127–128 ºC (yellow solid). IR ν_{max} 3004.2, 2836.5, 1652.3, 1613.9, 1523.7, 1494.7, 1248.7 cm^{-1}. NMR ^1H (300 MHz, $CDCl_3$) δ = 8.23 (s, 4 H), 7.30–7.11 (m, 5 H), 5,76 (s, 2 H), 2.24 (s, 3 H) ppm. NMR ^{13}C (75 MHz, $CDCl_3$) δ = 163.5 (C), 149.0 (C), 137.2 (C), 133.4 (C), 131.3 (C), 131.1 (CH), 130.2 (CH), 129.6 (CH), 127.7 (CH) 126.7 (CH), 124.3 (CH), 55.2 (CH_2), 19.4 (CH_3) ppm. HR ESMS *m/z* 296.1144 $(M+H)^+$. Calculated for $C_{15}H_{13}N_5O_2$: 296.1147.

2-(3-Methylbenzyl)− 5-(4-nitrophenyl)− 2*H*-tetrazole (4): yield = 52%; m.p. = 127–128 ºC (yellow solid). IR ν_{max} 3004.2, 2836.5, 1652.3, 1613.9, 1523.7, 1494.7, 1248.7 cm^{-1}. NMR ^1H (300 MHz, $CDCl_3$) δ = 8.24 (s, 4 H), 7.25–7.05 (m, 5 H), 5.71 (s, 2 H), 2.27 (s, 3 H) ppm. NMR ^{13}C (75 MHz, $CDCl_3$) δ = 163.6 (C), 149.0 (C), 139.2 (C), 133.4 (C), 132.8 (C), 130.1 (CH), 129.3 (CH), 129.2 (CH), 127.7 (CH), 125.7 (CH), 124.3 (CH), 57.3 (CH_2), 21.4 (CH_3) ppm. HR ESMS *m/z* 296.1150 $(M+H)^+$. Calculated for $C_{15}H_{13}N_5O_2$: 296.1147.

2-(4-Methylbenzyl)− 5-(4-nitrophenyl)− 2*H*-tetrazole (5): yield = 46%; m.p. = 164–165 ºC (orange solid). IR ν_{max} 3004.2, 2836.5, 1652.3, 1613.9, 1523.7, 1494.7, 1248.7 cm^{-1}. NMR ^1H (300 MHz, $CDCl_3$) δ = 8.32 (s, 4 H), 7.35 (d, *J*=6 Hz, 2 H), 7.20 (d, *J*=6 Hz, 2 H), 5.79 (s, 2 H), 2.35 (s, 3 H) ppm. NMR ^{13}C (75 MHz, $CDCl_3$) δ = 163.7 (C), 149.0 (C), 139.4 (C), 133.4 (C), 130.0 (C), 129.8 (CH), 128.7 (CH), 127.7 (CH), 124.3 (CH), 57.2 (CH_2), 21.3 (CH_3) ppm. HR ESMS *m/z* 296.1143 $(M+H)^+$. Calculated for $C_{15}H_{13}N_5O_2$: 296.1147.

2-(2-Methoxybenzyl)− 5-(4-nitrophenyl)− 2*H*-tetrazole (6): yield = 41%; m.p. = 148–149 ºC (white solid). IR ν_{max} 3004.2, 2836.5, 1652.3, 1613.9, 1523.7, 1494.7, 1248.7, 1213.6 cm^{-1}. NMR ^1H (300 MHz, $CDCl_3$) δ = 8.23 (s, 4 H), 7.29 (td, *J*=6, 3 Hz, 1 H), 7.17 (dd, *J*=6, 3 Hz, 1 H), 6.93–6.83 (m, 2 H), 5.79 (s, 2 H), 3.78 (s, 3 H) ppm. NMR ^{13}C (75 MHz, $CDCl_3$) δ = 163.3 (C), 157.5 (C), 148.8 (C), 133.6 (C), 130.7 (CH), 130.3 (CH), 127.7 (CH), 124.3 (CH), 121.4 (C), 120.9 (CH), 111.0 (CH), 55.7 (CH_3), 52.3 (CH_2) ppm. HR ESMS *m/z* 334.0913 $(M+Na)^+$. Calculated for $C_{15}H_{13}N_5O_3$: 334.0916.

2-(3-Methoxybenzyl)− 5-(4-nitrophenyl)− 2*H*-tetrazole (7): yield = 58%; m.p. = 132–133 ºC (light brown solid). IR ν_{max} 3004.2, 2836.5, 1652.3, 1613.9, 1523.7, 1494.7, 1248.7, 1213.6 cm^{-1}. NMR ^1H (300 MHz, $CDCl_3$) δ = 8.32 (s, 4 H), 7.31 (t, *J*=6 Hz, 1 H), 7.01 (d, *J*=6 Hz, 1 H), 6.96–6.88 (m, 2 H), 5.80 (s, 2 H), 3.80 (s, 3 H) ppm. NMR ^{13}C (75 MHz, $CDCl_3$) δ = 163.7 (C), 160.2 (C), 149.0 (C), 134.4 (C), 133.4 (C), 130.4 (CH), 127.8 (CH), 124.3 (CH), 120.8 (CH), 114.6 (CH), 114.3 (CH), 57.3 (CH_2), 55.4 (CH_3) ppm. HR ESMS *m/z* 334.0921 $(M+Na)^+$. Calculated for $C_{15}H_{13}N_5O_3$: 334.0916.

2-(4-Methoxybenzyl)− 5-(4-nitrophenyl)− 2*H*-tetrazole (8): yield= 32%; m.p. = 157–158 ºC (light brown solid). IR ν_{max} 3004.2, 2836.5, 1652.3, 1613.9, 1523.7, 1494.7, 1248.7, 1213.6 cm^{-1}. NMR ^1H (300 MHz, $CDCl_3$) δ = 8.31 (s, 4 H), 7.40 (d, *J*=9 Hz, 2 H), 6.90 (d, *J*=9 Hz, 2 H), 5.76 (d, 2 H), 3.80 (s, 3 H) ppm. NMR ^{13}C (75 MHz, $CDCl_3$) δ = 163.6 (C), 160.4 (C), 149.0 (C), 133.4 (C), 130.3 (CH), 127.7 (CH), 125.0 (C), 124.3 (CH), 114.6 (CH), 56.8 (CH_2), 55.5 (CH_3) ppm. HR ESMS *m/z* 334.0924 $(M+Na)^+$. Calculated for $C_{15}H_{13}N_5O_3$: 334.0916.

2-(2-Bromobenzyl)− 5-(4-nitrophenyl)− 2*H*-tetrazole (9): yield = 23%; m.p. = 164–165 ºC (yellow solid). IR ν_{max} 3004.2, 2836.5, 1652.3, 1613.9, 1523.7, 1494.7, 1248.7, 588.2 cm^{-1}. NMR ^1H (300 MHz, $CDCl_3$) δ = 8.33 (s, 4 H), 7.65 (dd, *J*=9, 3 Hz, 1 H), 7.34 (td, *J*=9, 3 Hz, 1 H), 7.28–7.22 (m, 2 H), 5.98 (s, 2 H) ppm. NMR ^{13}C (75 MHz, $CDCl_3$) δ = 163.7 (C), 149.1 (C), 133.6 (CH), 133.3 (C), 132.6 (C), 130.8 (CH), 130.6 (CH), 128.3 (CH), 127.8 (CH), 124.3 (CH), 123.9 (C), 57.0 (CH_2) ppm. HR ESMS *m/z* 360.0095 $(M+H)^+$. Calculated for $C_{14}H_{10}BrN_5O_2$: 360.0096.

2-(3-Bromobenzyl)− 5-(4-nitrophenyl)− 2*H*-tetrazole (10): yield = 39%; m.p. = 133–134 ºC (yellow solid). IR ν_{max} 3004.2, 2836.5, 1652.3, 1613.9, 1523.7, 1494.7, 1248.7, 588.2 cm^{-1}. NMR ^1H (300 MHz, $CDCl_3$) δ = 8.33 (s, 4 H), 7.60 (apparent t, 1 H), 7.52 (dt, *J*=9, 3 Hz, 1 H), 7.37 (d, *J*=6 Hz, 1 H), 7.33 (t, *J*=6 Hz, 1 H), 5.80 (s, 2 H) ppm. NMR ^{13}C (75 MHz, $CDCl_3$) δ = 163.9 (C), 149.2 (C), 135.0 (C), 133.5 (C), 132.6 (CH), 131.7 (CH), 130.8 (CH), 127.9 (CH), 127.3 (C), 124.3 (CH), 123.2 (C), 56.5 (CH_2) ppm. HR ESMS *m/z* 360.0094 $(M+H)^+$. Calculated for $C_{14}H_{10}BrN_5O_2$: 360.0096.

2-(4-Bromobenzyl)− 5-(4-nitrophenyl)− 2*H*-tetrazole (11): yield = 17%; m.p. = 152–153 ºC (yellow solid). IR ν_{max} 3004.2, 2836.5, 1652.3, 1613.9, 1523.7, 1494.7, 1248.7, 588.2 cm^{-1}. NMR ^1H (300 MHz, $CDCl_3$) δ = 8.33 (s, 4 H), 7.53 (d, *J*=9 Hz, 2 H), 7.33 (d, *J*=9 Hz, 2 H), 5.78 (s, 2 H) ppm. NMR ^{13}C (75 MHz, $CDCl_3$) δ = 163.8 (C), 149.1 (C), 133.3 (C), 132.5 (CH), 131.8 (C), 130.4 (CH), 127.7 (CH), 124.3 (CH), 123.7 (C), 56.6 (CH_2) ppm. HR ESMS *m/z* 360.0094 $(M+H)^+$. Calculated for $C_{14}H_{10}BrN_5O_2$: 360.0096.

2-(2-Chlorobenzyl)− 5-(4-nitrophenyl)− 2*H*-tetrazole (12): yield = 12%; m.p. = 149–150 ºC (orange solid). IR ν_{max} 3004.2, 2836.5, 1652.3, 1613.9, 1523.7, 1494.7, 1248.7, 746.4 cm^{-1}. NMR ^1H (300 MHz, $CDCl_3$) δ = 8.33 (s, 4 H), 7.47 (dd, *J*=6, 3 Hz, 1 H), 7.38–7.28 (m, 3 H), 5.98 (s, 2 H) ppm. NMR ^{13}C (75 MHz, $CDCl_3$) δ = 163.7 (C), 149.1 (C), 134.1 (C), 133.3 (C), 130.8 (C), 130.7 (CH), 130.6 (CH), 130.3 (CH), 127.8 (CH), 127.6 (CH), 124.3 (CH), 54.5 (CH_2) ppm. HR ESMS *m/z* 316.0600 $(M+H)^+$. Calculated for $C_{14}H_{10}ClN_5O_2$: 316.0601.

2-(3-Chlorobenzyl)− 5-(4-nitrophenyl)− 2*H*-tetrazole (13): yield = 52%; m.p. = 125–126 ºC (yellow solid). IR ν_{max} 3004.2, 2836.5, 1652.3, 1613.9, 1523.7, 1494.7, 1248.7, 746.4 cm^{-1}. NMR ^1H (300 MHz, $CDCl_3$) δ = 8.32 (s, 4 H), 7.45–7.30 (m, 4 H), 5.81 (s, 2 H) ppm. NMR ^{13}C (75 MHz, $CDCl_3$) δ = 163.8 (C), 149.0 (C), 135.3 (C), 134.7 (C), 133.3 (C), 130.5 (CH), 129.6 (CH), 128.8 (CH), 127.8 (CH), 126.7 (CH), 124.4 (CH), 56.5 (CH_2) ppm. HR ESMS *m/z* 316.0598 $(M+H)^+$. Calculated for $C_{14}H_{10}ClN_5O_2$: 316.0601.

2-(4-Chlorobenzyl)− 5-(4-nitrophenyl)− 2*H*-tetrazole (14): yield = 59%; m.p. = 150–151 ºC (yellow solid). IR ν_{max} 3004.2, 2836.5, 1652.3, 1613.9, 1523.7, 1494.7, 1248.7, 746.4 cm^{-1}. NMR ^{1}H (300 MHz, $CDCl_3$) δ = 8.33 (s, 4 H), 7.38 (s, 4 H), 5.80 (s, 2 H) ppm. NMR ^{13}C (75 MHz, $CDCl_3$) δ = 163.7 (C), 149.0 (C), 135.5 (C), 133.4 (C), 131.4 (C), 130.1 (CH), 129.5 (CH), 127.7 (CH), 124.3 (CH), 56.5 (CH_2) ppm. HR ESMS *m/z* 316.0593 $(M+H)^+$. Calculated for $C_{14}H_{10}ClN_5O_2$: 316.0601.

*2.1.1.5. Synthesis and characterization of tetrazole derivatives **15–27**.* Zn powder (147 eq.) was added to a solution of the corresponding nitrotetrazole derivative (1 eq.) in glacial AcOH (32.6 mL/mmol). The reaction mixture was vigorously stirred at room temperature preserved from light for 1 h. Next, the reaction was filtered over Celite and the filtration residue was thoroughly washed with ethyl acetate. The filtrate was neutralized using an aqueous saturated solution of $NaHCO_3$ and Na_2CO_3 until basic pH (10−11). The aqueous phase was extracted three times with ethyl acetate (3 ×10 mL) and the collected organic phases were washed with brine and dried over anhydrous $MgSO_4$. After solvent elimination under vacuum the residue was purified by column chromatography on silica gel using a hexane:ethyl acetate (1:1) mixture.

4-(2-Benzyl-2*H*-tetrazol-5-yl)aniline (15): yield = 71%; m.p. = 137–138 ºC (light brown solid). IR ν_{max} 3309.9, 3205.5, 3004.2, 2836.5, 1652.3, 1613.9, 1494.7, 1248.7 cm^{-1}. NMR ^{1}H (400 MHz, DMSO-d_6) δ = 7.69 (d, *J*=8 Hz, 2 H), 7.43–7.33 (m, 5 H), 6.65 (d, *J*=8 Hz, 2 H), 5.90 (s, 2 H), 5.57 (broad s, 2 H) ppm. NMR ^{13}C (100 MHz, DMSO-d_6) δ = 164.8 (C), 150.9 (C), 134.3 (C), 128.7 (CH), 128.4 (CH), 128.2 (CH), 127.5 (CH), 113.7 (C), 113.6 (CH), 55.7 (CH_2) ppm. HR ESMS *m/z* 252.1253 $(M+H)^+$. Calculated for $C_{14}H_{13}N_5$: 252.1249.

4-(2-(2-Methylbenzyl)− 2*H*-tetrazol-5-yl)aniline (16): yield = 93%; m.p. = 113–114 ºC (yellow solid). IR ν_{max} 3309.9, 3205.5, 3004.2, 2836.5, 1652.3, 1613.9, 1494.7, 1248.7 cm^{-1}. NMR ^{1}H (400 MHz, DMSO-d_6) δ = 7.68 (d, *J*=8 Hz, 7.30–7.20 (m, 4 H), 6.65 (d, *J*=8 Hz, 2 H), 5.90 (s, 2 H), 5.57 (broad s, 2 H), 2.35 (s, 3 H) ppm. NMR ^{13}C (100 MHz, DMSO-d_6) δ = 165.0 (C), 150.8 (C), 136.8 (C), 132.5 (C), 130.5 (CH), 129.4 (CH), 128.7 (CH), 127.5 (CH), 126.2 (CH), 113.7 (C), 113.6 (CH), 54.0 (CH_2), 18.6 (CH_3) ppm. HR ESMS *m/z* 266.1400 $(M+H)^+$. Calculated for $C_{15}H_{15}N_5$: 266.1406.

4-(2-(3-Methylbenzyl)− 2*H*-tetrazol-5-yl)aniline (17): yield = 46 %; m.p. = 112–114 ºC (orange solid). IR ν_{max} 3309.9, 3205.5, 3004.2, 2836.5, 1652.3, 1613.9, 1494.7, 1248.7 cm^{-1}. NMR ^{1}H (400 MHz, DMSO-d_6) δ = 7.69 (d, *J*=8 Hz, 2 H), 7.28 (t, *J*=8 Hz, 2 H), 7.19–7.14 (m, 3 H), 6.65 (d, *J*=8 Hz, 2 H), 5.85 (s, 2 H), 5.59 (broad s, 2 H), 2.28 (s, 3 H) ppm. NMR ^{13}C (100 MHz, DMSO-d_6) δ = 165.2 (C), 150.9 (C), 138.1 (C), 134.3 (C), 129.2 (CH), 128.8 (CH), 128.7 (CH), 127.5 (CH), 125.3 (CH), 113.7 (C), 113.6 (CH), 55.7 (CH_2), 20.9 (CH_3) ppm. HR ESMS *m/z* 266.1409 $(M+H)^+$. Calculated for $C_{15}H_{15}N_5$: 266.1406.

4-(2-(4-Methylbenzyl)− 2*H*-tetrazol-5-yl)aniline (18): yield = 63 %; m.p. = 117–118 ºC (light brown solid). IR ν_{max} 3309.9, 3205.5, 3004.2, 2836.5, 1652.3, 1613.9, 1494.7, 1248.7 cm^{-1}. NMR ^{1}H (400 MHz, DMSO-d_6) δ = 7.68 (d, *J*=8 Hz, 2 H), 7.27 (d, *J*=8 Hz, 2 H), 7.19 (d, *J*=8 Hz, 2 H), 6.65 (d, *J*=8 Hz, 2 H), 5.83 (s, 2 H), 5.58 (broad s, 2 H), 2.28 (s, 3 H) ppm. NMR ^{13}C (100 MHz, DMSO-d_6) δ = 165.2 (C), 150.8 (C), 137.9 (C), 131.4 (C), 129.4 (CH), 128.2 (CH), 127.4 (CH), 113.8 (C), 113.7 (CH), 55.5 (CH_2), 20.7 (CH_3) ppm. HR ESMS *m/z* 266.1408 $(M+H)^+$. Calculated for $C_{15}H_{15}N_5$: 266.1406.

4-(2-(2-Methoxybenzyl)− 2*H*-tetrazol-5-yl)aniline (19): yield = 58%; m.p. = 141–142 ºC (white solid). IR ν_{max} 3309.9, 3205.5, 3004.2, 2836.5, 1652.3, 1613.9, 1494.7, 1248.7, 1213.6 cm^{-1}. NMR ^{1}H (400 MHz, DMSO-d_6) δ = 7.68 (d, *J*=8 Hz, 2 H), 7.37 (td, *J*=8, 4 Hz, 1 H), 7.23 (dd, *J*=8, 4 Hz, 1 H), 7.07 (dd, *J*=8, 1 Hz, 1 H), 6.97 (td, *J*=8, 1 Hz, 1 H), 5.80 (s, 2 H), 5.55 (broad s, 2 H), 3.78 (s, 3 H) ppm. NMR ^{13}C (100 MHz, DMSO-d_6) δ = 164.8 (C), 157.1 (C), 150.5 (C), 130.3 (CH), 130.2 (CH), 127.5 (CH), 121.8 (C), 120.5 (CH), 114.0 (C), 113.8 (CH), 111.3 (CH), 55.6 (CH_3), 51.2 (CH_2) ppm. HR ESMS *m/z* 282.1348 $(M+H)^+$. Calculated for $C_{15}H_{15}N_5O$: 282.1355.

4-(2-(3-Methoxybenzyl)− 2*H*-tetrazol-5-yl)aniline (20): yield = 82%; m.p. = 88–89 ºC (orange solid). IR ν_{max} 3309.9, 3205.5, 3004.2, 2836.5, 1652.3, 1613.9, 1494.7, 1248.7, 1213.6 cm^{-1}. NMR ^{1}H (400 MHz, DMSO-d_6) δ = 7.70 (d, *J*=8 Hz, 2 H), 7.31 (t, *J*=8 Hz, 1 H), 6.97–6.87 (m, 3 H), 6.66 (d, *J*=8 Hz, 2 H), 5.87 (s, 2 H), 5.57 (broad s), 3.74 (s, 3 H) ppm. NMR ^{13}C (100 MHz, DMSO-d_6) δ = 165.1 (C), 159.4 (C), 150.9 (C), 135.8 (C), 129.9 (CH), 127.5 (CH), 120.2 (CH), 113.9 (CH), 113.8 (CH), 113.7 (C), 113.6 (CH), 55.6 (CH_2), 55.1 (CH_3) ppm. HR ESMS *m/z* 282.1357 $(M+H)^+$. Calculated for $C_{15}H_{15}N_5O$: 282.1355.

4-(2-(4-Methoxybenzyl)− 2*H*-tetrazol-5-yl)aniline (21): yield = 62%; m.p. = 124–126 ºC (light brown solid). IR ν_{max} 3309.9, 3205.5, 3004.2, 2836.5, 1652.3, 1613.9, 1494.7, 1248.7, 1213.6 cm^{-1}. NMR ^{1}H (400 MHz, DMSO-d_6) δ = 7.68 (d, *J*=8 Hz, 2 H), 7.35 (d, *J*=8 Hz, 2 H), 6.95 (d, *J*=8 Hz, 2 H), 6.65 (d, *J*=8 Hz, 2 H), 5.80 (s, 2 H), 5.56 (broad s, 2 H), 3.74 (s, 3 H) ppm. NMR ^{13}C (100 MHz, DMSO-d_6) δ = 165.1 (C), 159.2 (C), 150.8 (C), 129.8 (C), 127.5 (CH), 126.2 (C), 114.3 (CH), 113.8 (C), 113.7 (CH), 55.3 (CH_2), 55.2 (CH_3) ppm. HR ESMS *m/z* 282.1359 $(M+H)^+$. Calculated for $C_{15}H_{15}N_5O$: 282.1355.

4-(2-(2-Bromobenzyl)− 2*H*-tetrazol-5-yl)aniline (22): yield = 86%; m.p. = 122–124 ºC (yellow solid). IR ν_{max} 3309.9, 3205.5, 3004.2, 2836.5, 1652.3, 1613.9, 1494.7, 1248.7, 588.2 cm^{-1}. NMR ^{1}H (400 MHz, $CDCl_3$) δ = 7.95 (d, *J*=8 Hz, 2 H), 7.62 (dd, *J*=8, 1 Hz, 1 H), 7.28 (td, *J*=8, 1 Hz, 1 H), 7.21(td, *J*=8, 1 Hz, 1 H), 7.08 (dd, *J*=8, 1 Hz, 1 H), 6.73 (d, *J*=8 Hz, 2 H), 5.93 (s, 2 H), 3.9 (broad s, 2 H) ppm. NMR ^{13}C (100 MHz, $CDCl_3$) δ = 165.8 (C), 148.6 (C), 133.4 (C), 133.3 (CH), 130.4 (CH), 129.9 (CH), 128.5 (CH), 128.1 (CH), 123.4 (C), 117.5 (C), 115.0 (CH), 56.4 (CH_2) ppm. HR ESMS *m/z* 330.0352 $(M+H)^+$. Calculated for $C_{14}H_{12}BrN_5$: 330.0354.

4-(2-(3-Bromobenzyl)− 2*H*-tetrazol-5-yl)aniline (23): yield = 86%; m.p. = 122–124 ºC (yellow solid). IR ν_{max} 3309.9, 3205.5, 3004.2, 2836.5, 1652.3, 1613.9, 1494.7, 1248.7, 588.2 cm^{-1}. NMR ^{1}H (400 MHz, DMSO-d_6) δ = 7.70 (d, *J*=8 Hz, 2 H), 7.63 (apparent s, 1 H), 7.59–7.56 (m, 1 H), 7.37 (d, *J*=8 Hz, 2 H), 6.66 (d, *J*=8 Hz, 2 H), 5.93 (s, 2 H), 5.59 (broad s, 2 H) ppm. NMR ^{13}C (100 MHz, DMSO-d_6) δ = 165.3 (C), 151.0 (C), 136.8 (C), 131.4 (CH), 131.0 (CH), 130.9 (CH), 127.5 (CH), 127.3 (CH), 121.8 (C), 113.7 (CH), 113.6 (C), 54.7 (CH_2) ppm. HR ESMS *m/z* 330.0352 $(M+H)^+$. Calculated for $C_{14}H_{12}BrN_5$: 330.0354.

4-(2-(4-Bromobenzyl)− 2*H*-tetrazol-5-yl)aniline (24): yield = 59%; m.p. = 110–112 ºC (orange solid). IR ν_{max} 3309.9, 3205.5, 3004.2, 2836.5, 1652.3, 1613.9, 1494.7, 1248.7, 588.2 cm^{-1}. NMR ^{1}H (400 MHz, DMSO-d_6) δ = 7.68 (d, *J*=8 Hz, 2 H), 7.60 (d, *J*=8 Hz, 2 H), 7.34 (d, *J*=8 Hz, 2 H), 6.65 (d, *J*=8 Hz, 2 H), 5.90 (s, 2 H), 5.58 (broad s, 2 H) ppm. NMR ^{13}C (100 MHz, DMSO-d_6) δ = 165.3 (C), 150.9 (C), 133.8 (C), 131.7 (CH), 130.5 (CH), 127.5 (CH), 121.7 (C), 113.6 (CH), 113.5 (C), 55.0 (CH_2) ppm. HR ESMS *m/z* 330.0354 $(M+H)^+$. Calculated for $C_{14}H_{12}BrN_5$: 330.0354.

4-(2-(2-Chlorobenzyl)− 2*H*-tetrazol-5-yl)aniline (25): yield = 48%; m.p. = 129–131 ºC (yellow solid). IR ν_{max} 3309.9, 3205.5, 3004.2, 2836.5, 1652.3, 1613.9, 1494.7, 1248.7, 746.4 cm^{-1}. NMR ^{1}H (400 MHz, DMSO-d_6) δ = 7.67 (d, *J*=8 Hz, 2 H), 7.56–7.52 (m, 1 H), 7.47–7.37 (m, 3 H), 6.65 (d, *J*=8 Hz, 2 H), 5.98 (s, 2 H), 5.58 (broad s, 2 H) ppm. NMR ^{13}C (100 MHz, DMSO-d_6) δ = 165.0 (C), 150.9 (C), 133.1 (C), 131.5 (C), 131.4 (CH), 130.6 (CH), 129.7 (CH), 127.7 (CH), 127.5 (CH), 113.7 (CH), 113.6 (C), 53.7 (CH_2) ppm. HR ESMS *m/z* 286.0852 $(M+H)^+$. Calculated for $C_{14}H_{12}ClN_5$: 286.0859.

4-(2-(3-Chlorobenzyl)− 2*H*-tetrazol-5-yl)aniline (26): yield = 93%; m.p. = 104–105 ºC (yellow solid). IR ν_{max} 3309.9, 3205.5, 3004.2, 2836.5, 1652.3, 1613.9, 1494.7, 1248.7, 746.4 cm^{-1}. NMR ^{1}H (400 MHz, DMSO-d_6) δ = 7.71 (d, *J*=8 Hz, 2 H), 7.48 (apparent s, 1 H), 7.44–7.41 (m, 2 H), 7.34–7.31 (m, 1 H), 6.68 (d, *J*=8 Hz, 2 H), 5.93 (s, 2 H), 5.60 (broad s, 2 H) ppm. NMR ^{13}C (100 MHz, DMSO-d_6) δ = 165.3 (C), 151.0 (C), 136.6 (C), 133.2 (C), 130.7 (CH), 128.5 (CH), 128.2 (CH), 127.5 (CH), 126.8 (CH), 113.7 (CH), 113.6 (C), 54.8 (CH_2) ppm. HR ESMS *m/z* 286.0860 $(M+H)^+$. Calculated for $C_{14}H_{12}ClN_5$: 286.0859.

4-(2-(4-Chlorobenzyl)− 2*H*-tetrazol-5-yl)aniline (27): yield= 75%; m.p. = 112–113 ºC (yellow solid). IR ν_{max} 3309.9, 3205.5, 3004.2, 2836.5, 1652.3, 1613.9, 1494.7, 1248.7, 746.4 cm^{-1}. NMR ^{1}H (400 MHz, DMSO-d_6) δ = 7.68 (d, *J*=8 Hz, 2 H), 7.47 (d, *J*=8 Hz, 2 H), 7.40 (d, *J*=8 Hz, 2 H), 6.65 (d, *J*=8 Hz, 2 H), 5.93 (s, 2 H), 5.59 (broad s, 2 H) ppm. NMR ^{13}C (100 MHz, DMSO-d_6) δ = 165.3 (C), 151.0 (C), 133.4 (C), 133.2 (C), 130.3 (CH), 128.8 (CH), 127.5 (CH), 113.7 (CH), 113.6 (C), 54.8 (CH_2) ppm. HR ESMS *m/z* 286.0863 $(M+H)^+$. Calculated for $C_{14}H_{12}ClN_5$: 286.0859.

2.1.2. Biological studies

2.1.2.1. Cell culture. Cell culture media were purchased from Gibco (Grand Island, NY). Fetal bovine serum (FBS) was obtained from Harlan-Seralab (Belton, U.K.). Supplements and other chemicals not listed in this section were obtained from Sigma Chemical Co. (St. Louis, MO). Plastics for cell culture were supplied by Thermo Scientific BioLite. All tested compounds were dissolved in DMSO at a concentration of 20 mM and stored at − 20 °C until use.

HT-29, A549, MCF-7 and HEK-293 cell lines were maintained in Dulbecco's modified Eagle's medium (DMEM) containing glucose (1 g/L), glutamine (2 mM), penicillin (50 μg/mL), streptomycin (50 μg/mL), and amphotericin B (1.25 μg/mL), supplemented with 10% FBS.

2.1.2.2. Cell proliferation assay. In 96-well plates, 5×10^3 cells per well were incubated with serial dilutions of the tested compounds in a total volume of 100 μL of their growth media. The 3-(4,5-dimethylthiazol-2-yl)− 2,5-diphenyltetrazolium bromide (MTT; Sigma Chemical Co.) dye reduction assay in 96-well microplates was used. After 2 days of incubation (37 °C, 5% CO_2 in a humid atmosphere), 10 μL of MTT (5 mg/mL in phosphate-buffered saline, PBS) was added to each well, and the plate was incubated for a further 3 h (37 °C). After that, the supernatant was discarded and replaced by 100 μL of DMSO to dissolve formazan crystals. The absorbance was then read at 550 nm by spectro-photometry. For all concentrations of compound, cell viability was expressed as the percentage of the ratio between the mean absorbance of treated cells and the mean absorbance of untreated cells. Three independent experiments were performed, and the IC_{50} values (i.e., concentration half inhibiting cell proliferation) were graphically determined using GraphPad Prism 4 software.

2.1.2.3. PD-L1, VEGFR-2, CD-47 and c-Myc relative quantification by Flow Cytometry. To study the effect of the compounds on every biological target in cancer cell lines compounds were used at 100 μM or 10 μM. For the assay, 10^5 cells per well were incubated for 48 h with the corresponding dose of the tested compound in a total volume of 500 μL of their growth media. To detect membrane PD-L1, VEGFR-2 and CD-47 after cell treatments, they were collected, fixed with 4% in PBS paraformaldehyde and stained with FITC Mouse monoclonal Anti-Human VEGFR-2 (ab184903), FITC Mouse monoclonal Anti-CD-47 (ab134484) and Alexa Fluor® 647 Rabbit monoclonal Anti-PD-L1 (ab215251). To detect c-Myc and total proteins, after fixing cells, and before adding antibody FITC Rabbit monoclonal Anti-c-Myc (ab223913), cells were treated with 0,5% in PBS TritonTM X-100.

2.1.2.4. Apoptosis Assay. To study the apoptotic activity of some of the compounds it was used BD Pharmingen™ FITC Annexin V Apoptosis Detection Kit I (Cat: 556547). Briefly, after collecting cells with acutase, they were resuspended in 1X Binding Buffer to obtain a concentration of 10^5 cells per mL. After that, to an aliquot of 100 μL was added 5 μL of Annexin-V-FITC and 5 μL of propidium iodide. Finally, apoptosis activity was measured by flow cytometry.

2.1.2.5. Cell viability evaluation in co-cultures. To study the effect of the compounds on cell viability in co-culture with THP-1 cells, 10^5 HT-29 cells line per well were seeded and incubated for 24 h. Then, medium was changed by a cell culture medium supplemented with IFN-γ (10 ng/mL; human, Invitrogen®) containing 5×10^5, 2.5×10^5, 10^5 or 5×10^4 of THP-1 cells per well and the corresponding compound at 100 μM or 10 μM. For the positive control DMSO was added. After 48 h of incubation, supernatants were collected to determine THP-1 living cells. Besides, stain cancer cells were collected with trypsin. Both types of suspension cells were fixed with 4% in PBS paraformaldehyde and counted by flow cytometry.

2.1.2.6. TNF-α secreted relative quantification by ELISA assay. To study the effect of the compounds on secreted TNF-α, 10^5 cells per well were incubated for 48 h with the corresponding dose of the tested compound in a total volume of 500 μL of their growth media. These media were collected and used as a sample in the Invitrogen® Human TNF-α ELISA Kit (Cat: KAC1751).

2.1.2.7. Statistical analysis. Statistical significance was evaluated using one-way ANOVA. Data were expressed as means ± SD for triplicates. The level of statistical significance differences was set as P values of $p < 0.05$.

3. Results

3.1. Synthesis of tetrazole derivatives 1-27

Tetrazole derivatives **1-14** were achieved upon ionization of 5-phenyl-2*H*-tetrazole or 5-(4-nitrophenyl)− 2*H*-tetrazole with NaH in CH_3CN, followed by reaction with a set of benzyl halides in the presence of catalytic amounts of NaI (see Scheme 1).

Reduction of tetrazoles **1–14** with Zn powder in glacial AcOH afforded the tetrazoles **15–27** (see Scheme 2).

All compounds were purified by column chromatography and characterized by ^{1}H and ^{13}C NMR, IR and Mass Spectrometry.

3.2. Study of the antiproliferative activity of tetrazole derivatives

The effect of the synthetized compounds **1-27** on cell proliferation was studied by MTT assay which allowed IC_{50} values calculation. The tested cell lines were HT-29 (human colon adenocarcinoma), A-549 (human lung adenocarcinoma), MCF-7 (human breast adenocarcinoma) and HEK-293 (human embryonic kidney cells). Most of the compounds were inactive below 100 μM. Table 1 shows the IC_{50} values obtained for the most active derivatives.

3.3. Study of the effect on PD-L1, CD-47, VEGFR-2 and c-Myc on HT-29

The aim of this study was to screen the synthetized compounds according to their effect on the expression of immune checkpoints PD-L1 and CD-47 that play an important role in defining the tumor microenvironment, VEGFR-2, that is key in the cancer promoted angiogenesis and c-Myc, which has been considered the master regulator of TME. The study was performed on HT-29 cell line by flow cytometry and the relative presence of PD-L1, CD-47 and VEGFR-2 on cell surface was also determined. Compounds were tested at 100 μM dose. Tables 2.1 and 2.2 show those compounds that exhibited any effect on the above mentioned targets and their relative amount compared to control (non-treated cells). The rest of the compounds were not active. Representative plots of compounds **26** and **27** are included in Supporting Information.

To check the dose-effect dependency, we selected chloro derivatives **25-27**. The effect on all the biological targets was studied at 10 μM dose (see Table 3). We observed no inhibition of c-Myc and a very mild effect on PD-L1 and VEGFR-2. In the case of CD-47, around 20% of protein inhibition in the surface of HT-29 cells and around 30% of inhibition of total CD-47 were measured.

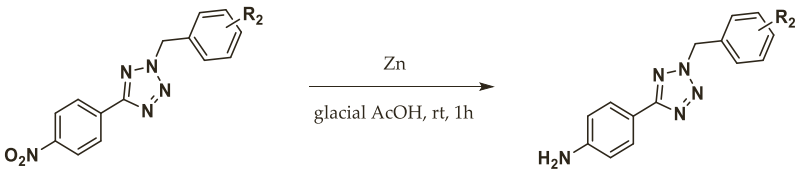

15	(71%)	R_2 = H	**22**	(86%)	R_2 = *o*-Br
16	(93%)	R_2 = *o*-CH_3	**23**	(41%)	R_2 = *m*-Br
17	(46%)	R_2 = *m*-CH_3	**24**	(59%)	R_2 = *p*-Br
18	(63%)	R_2 = *p*-CH_3	**25**	(48%)	R_2 = *o*-Cl
19	(58%)	R_2 = *o*-OCH_3	**26**	(93%)	R_2 = *m*-Cl
20	(82%)	R_2 = *m*-OCH_3	**27**	(75%)	R_2 = *p*-Cl
21	(62%)	R_2 = *p*-OCH_3			

Scheme 2. Synthesis of functionalized tetrazoles **15–27**.

Table 1
IC_{50} values (μM) for the reference compounds and the most active ones. Data are expressed as means ± SD for triplicates.

	HT-29	A-549	MCF-7	HEK-293
5	66 ± 5	33 ± 17	35 ± 6	> 100
12	8 ± 2	> 100	> 100	> 100
13	29 ± 13	> 100	> 100	> 100
17	> 100	94 ± 15	> 100	> 100
18	68 ± 7	54 ± 2	71 ± 5	59 ± 14
24	72 ± 4	38 ± 1	69 ± 6	> 100
27	60 ± 20	> 100	53 ± 7	> 100
Sorafenib	17 ± 4	27 ± 2	14 ± 4	5 ± 1
BMS-8	19 ± 2	6 ± 1	20 ± 3	60 ± 10

Table 2.1
Relative amount of mPD-L1, tPD-L1 and c-Myc compared to control (%) for the most active compounds at 100 μM. Data are expressed as means ± SD for triplicates.

HT-29 (48 h) (100 μM)			
Comp.	mPD-L1	tPD-L1	c-Myc
9	51 ± 9	> 100	> 100
10	99 ± 3	> 100	> 100
11	> 100	> 100	> 100
12	66 ± 15	> 100	> 100
13	94 ± 2	> 100	55 ± 16
14	> 100	> 100	> 100
22	97 ± 6	> 100	72 ± 6
23	95 ± 5	> 100	51 ± 1
24	96 ± 3	> 100	47 ± 11
25	97 ± 6	55 ± 9	81 ± 3
26	98 ± 9	48 ± 7	72 ± 5
27	> 100	49 ± 15	62 ± 4

3.4. Study of the effect on apoptosis in HT-29 for selected haloderivatives

The aim of this study was to determine whether the most active derivatives were able to promote apoptosis in HT-29 cells. The results of the assay using Annexin V conjugated to FITC and propidium iodide are depicted in Fig. 2. The study was performed for 24 h of treatment at 100 μM doses.

As it is shown in Fig. 2A all the selected chloro derivatives were able to enhance apoptosis, as about 70% of apoptotic cells versus 30% for non-treated ones (control cells) were found. Fig. 2B shows the morphological changes suffered by HT-29 cells after 48 h of treatment with 100 μM with the corresponding compounds. Cells showed typical apoptotic features such as nuclear fragmentation (i), membrane blebbing (ii), cellular shrinkage (iii), apoptotic bodies (iv) and nuclear condensation (v).

Table 2.2
Relative amount of mVEGFR-2, t-VEGFR-2 and mCD-47 compared to control (%) for the most active compounds at 100 μM. Data are expressed as means ± SD for triplicates.

HT-29 (48 h) (100 μM)			
Comp.	mVEGFR-2	tVEGFR-2	mCD-47
9	> 100	> 100	96 ± 6
10	> 100	91 ± 8	91 ± 12
11	> 100	> 100	86 ± 4
12	> 100	> 100	96 ± 1
13	97 ± 0	96 ± 7	68 ± 20
14	> 100	> 100	90 ± 14
22	> 100	92 ± 16	95 ± 8
23	> 100	> 100	93 ± 6
24	> 100	> 100	88 ± 10
25	86 ± 2	> 100	91 ± 7
26	90 ± 11	> 100	94 ± 11
27	> 100	> 100	97 ± 5

Table 3
Relative amount of the tested targets compared to control (%) for compounds **25-27** at 10 μM after 48 h of treatment. Data are expressed as means ± SD for triplicates.

HT-29 (48 h) (10 μM)						
Comp.	mPD-L1	tPD-L1	mVEGFR-2	tVEGFR-2	mCD-47	tCD-47
25	99 ± 2	> 100	> 100	93 ± 9	84 ± 5	79 ± 26
26	92 ± 1	92 ± 20	> 100	78 ± 3	80 ± 2	69 ± 5
27	95 ± 3	96 ± 3	95 ± 5	96 ± 8	88 ± 4	69 ± 14

3.5. Study of the effect on HT-29 cell viability in co-culture with THP-1 monocytes

The aim of this study was to check the effect of our compounds on cell proliferation in a microenvironment similar to TME, that is cancer cells co-cultured in the presence of immune cells. In this study, we tested all the synthetized compounds at 100 μM for 48 h using a 1:5 proportion of cancer versus immune cells. Then, we determined by flow cytometry the cell viability of both cell population, HT-29 cells and THP-1 monocytes. Fig. 3 shows the relative amount of living cancer cells related to control or non-treated cells. Thus, *p*-nitro derivatives, in general, are less effective in inhibiting cancer cell proliferation in co-cultures than the *p*-amine ones. *m*-methyl **4** and *m*-methoxy **7** are the most active of nitro derivatives, showing inhibition rates of around 75%. On the other hand, *o*-methyl **16**, *m*-methyl **17** and halo derivatives **22-27** were the most active among the amine derivatives. The action of these compounds is especially relevant provoking more than 95% of inhibition of cell proliferation, at a dose (100 μM) in which the antiproliferative effect was

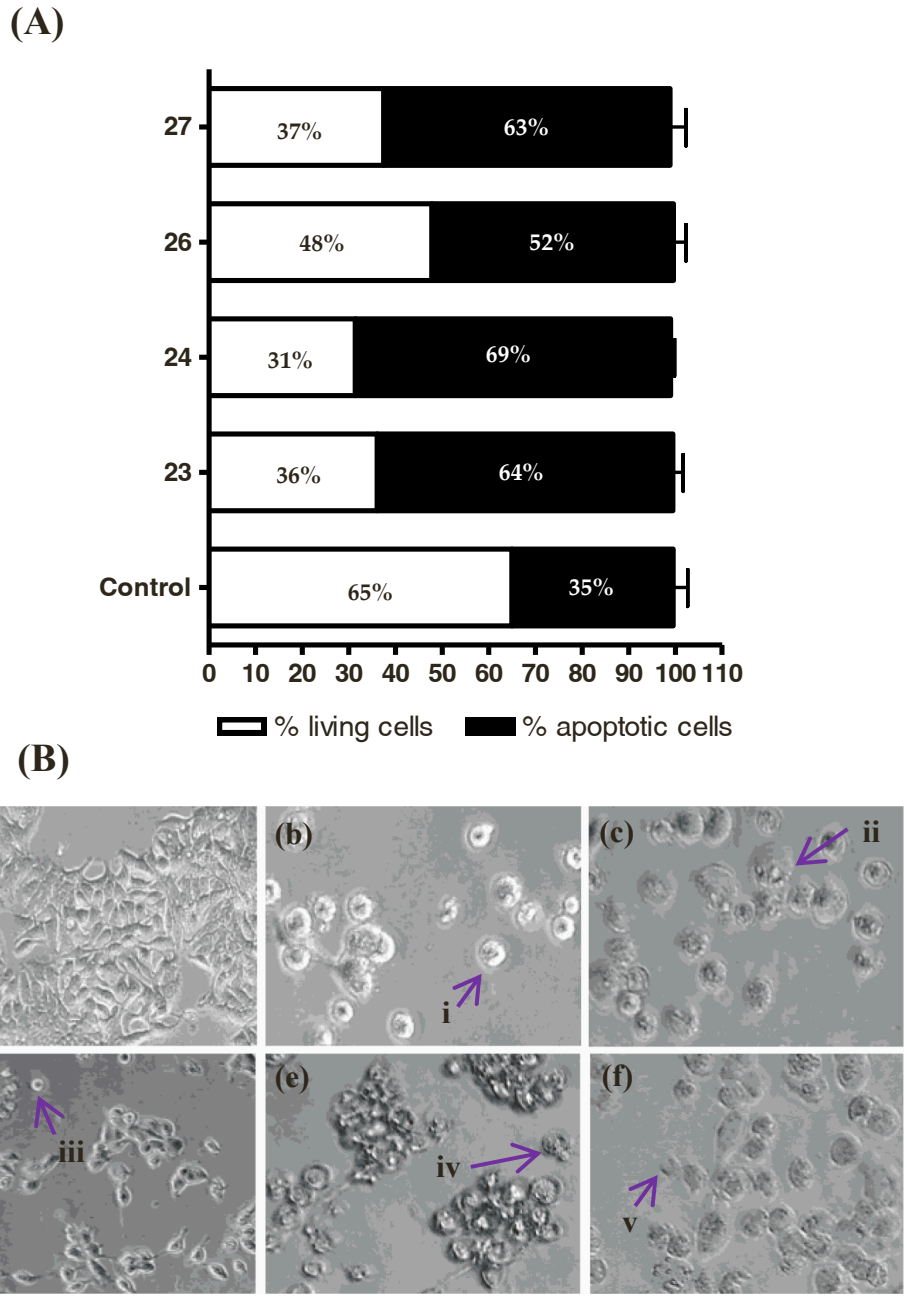

Fig. 2. A) Effect of selected compounds on apoptosis in HT-29 cells. Data are expressed as means ± SD for triplicates. B) Picture of HT-29 after 24 h of treatment with 100 μM doses of: (a) DMSO, (b) **23**, (c) **24**; (d) **25**, (e) **26** and (f) **27**. Arrows: i. Nuclear fragmentation, ii. Membrane blebbing, iii. Cellular shrinkage, iv. Apoptotic bodies, v. Nuclear compaction.

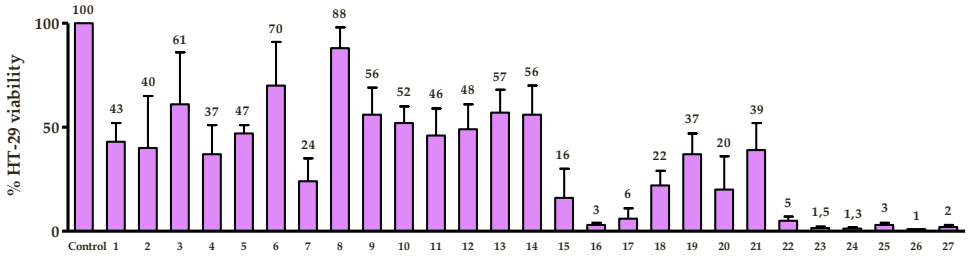

Fig. 3. Proportion of cancer living cells, HT-29, when co-cultured with monocytes THP-1, related to non-treated cells. Data are expressed as means ± SD for triplicates.

very mild in monocultures of HT-29. We also determined the proportion of monocytes living cells in the corresponding co-cultures (see Fig. 4). In this case we found a mild effect on inhibition of monocyte proliferation for most of the compounds but, in some cases, we found that amine derivatives, such as methyl ones, can stimulate the proliferation of these immune cells.

After these screening assay with all the synthetized compounds, we selected the most active compounds, **16**, **17**, **22-27** for a further study on HT-29 cell viability in co-culture with THP-1 monocytes. To study the influence of the proportion of cancer and immune cells we repeated the previous assay but instead of using a 1:5 proportion of cancer versus immune cell, we used 1:2.5, 1:1 and 2:1 proportion, and 100 μM and 10 μM doses of the corresponding compounds.

Fig. 5 shows the percentage of cancer living cells related to control for each compound at both doses. The percentage of immune living cells related to control for each compound at both doses are depicted in Fig. 5S (see Supporting Information).

Results show that at 100 μM doses, *m*- and *p*-halo derivatives **23**, **24**, **26** and **27** inhibited cancer cell proliferation without any dependence of cancer and immune cell proportion. After 48 h of co-cultures treatment with these compounds, we found less than 5% of cancer living cells compared to non-treated samples and no effect on immune cells. The rest of the tested compounds were still very active in inhibiting cancer cell proliferation with no effect on immune cells, as they show inhibition rates higher than 70% in all cases. It is worth mentioning that the best results were obtained for a 1:5 and 1:1 cancer versus immune cell proportions.

When these studies were performed at 10 μM doses we found that the effect was milder for each compound and proportion tested. In all the cases, we found that 2:1 cancer versus immune cell proportion was the worst conditions, with inhibition rates less than 20%. It is curious that 1:5 proportion was not the most effective but 1:1 and 1:2.5 were the ones that, in general, gave the best results. Compound **22** was the only one that exhibited the same effect without dependence of cancer and immune cell proportions yielding more than 40% of inhibition rates. The most effective compounds at 10 μM doses and cell proportions were **23**, **24**, **26** and **27** in a medium containing 1:2.5 proportion of cancer and immune cells. Finally, we selected chloro derivatives **25-27** to determine their IC_{50} values towards HT-29 in co-culture with different proportions of THP-1. This allowed us to determine that IC_{50} values were four to eight times higher than the ones obtained for HT-29 monocultures. Fig. 6 shows IC_{50} values for all the conditions (percentages of cancer living cells related to control can be seen in Fig. 6.1 S and 6.2 S of the Supporting information file).

3.6. Study of the effect on the biological targets PD-L1 and CD-47 on cancer cells co-cultured with THP-1 monocytes

The aim of this study was to check the effect of our compounds on the immune checkpoints PD-L1 and CD-47 in cancer cell membrane. We, again, took advantage of flow cytometry versatility to perform this study simultaneously to the previous one. Fig. 7 shows the relative amount of both proteins related to non-treated cells. All derivatives were tested at 100 μM. We can observe that, in general, compounds studied showed a moderated action in the inhibition of CD-47 expression on cell surface, while no effect was observed on PD-L1. Again, the amine derivatives were slightly more active than the nitro ones.

3.7. Study of the effect on the IL-6 and TNF-α secreted into the medium when co-cultured with THP-1 monocytes

We determined the effect of the halo derivatives **22-27** on the secretion of TNF-α in monocultures of HT-29 cells and in co-cultures of HT-29 and THP-1 (1:5 and 2:1 proportion). Assays were performed by ELISA using cell media after treatments with selected compounds at 100 μM for 48 h.

We used two very different proportions of cancer cells and monocytes (1:5 and 2:1) to make them more similar to those that can be found in TME. Results showed that TNF-α was not detected neither in any sample that came from cancer cell monocultures nor in control sample, while different quantities of this cytokine were measured for the samples that came from co-cultures of cancer cells and monocytes.

Table 4 shows the level of secreted TNF-α cytokine when co-cultures were treated with the selected compounds as well as the level of cytokine in control samples (non-treated co-culture cell medium).

We observed that in control samples the amount of TNF-α released into the media is higher as lower is the proportion of cancer cells related to monocytes. Thus, the amount of released TNF-α is almost ten times higher when the proportion HT-29/THP-1 was 1:5 compared to 2:1. For all the treated samples the levels of cytokine were higher than for the control samples. In the case of 1:5 proportion and for *ortho*-derivatives **22** and **25**, the level of TNF-α secreted into the medium was around 5 times higher than for non-treated co-cultures while it was around 2.5 times higher for *meta*-compounds **24** and **26** and 1.25 times higher for *para*-derivatives **23** and **27**. On the other hand, a different tendency was observed when cancer cells were in higher proportion than monocytes, and we found that **22** and **25** exhibited levels of TNF-α that were around 25 times higher than the control. For compounds **23**, **24**, **26** and **27** levels higher than 40 times related to control were measured.

We also measured, by ELISA, the levels of IL-6 secreted into the cell media of co-cultures of HT-29 and THP-1 (1:5 proportion) after treatments with the selected compounds at 100 μM for 48 h. Results are depicted in Table 4S in the Supporting Information and showed that these compounds had no effect on this cytokine secretion.

3.8. Study of the effect on monocultures of THP-1

The aim of this was to study by flow cytometry the effect of the chloro derivatives **25-27** on monocytes viability at 100 and 10 μM doses and also to study the effect of these compounds on cell proliferation in a microenvironment similar to TME, that is in THP-1 monocultures (see Fig. 8).

The relative amount of PD-L1 in treated monocytes compared to control cells was also stablished. In this sense we observed that at 100 μM concentration compounds inhibited more than 70% the expression of surface PD-L1 while at 10 μM the effect is still good as inhibition rates around 40% for compounds **26** and **27** were measured.

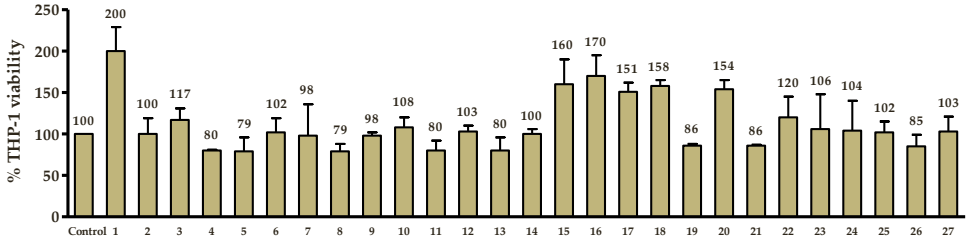

Fig. 4. Proportion of immune living cells, THP-1, in co-cultures of cancer cells, HT-29 related to non-treated cells. Data are expressed as means ± SD for triplicates.

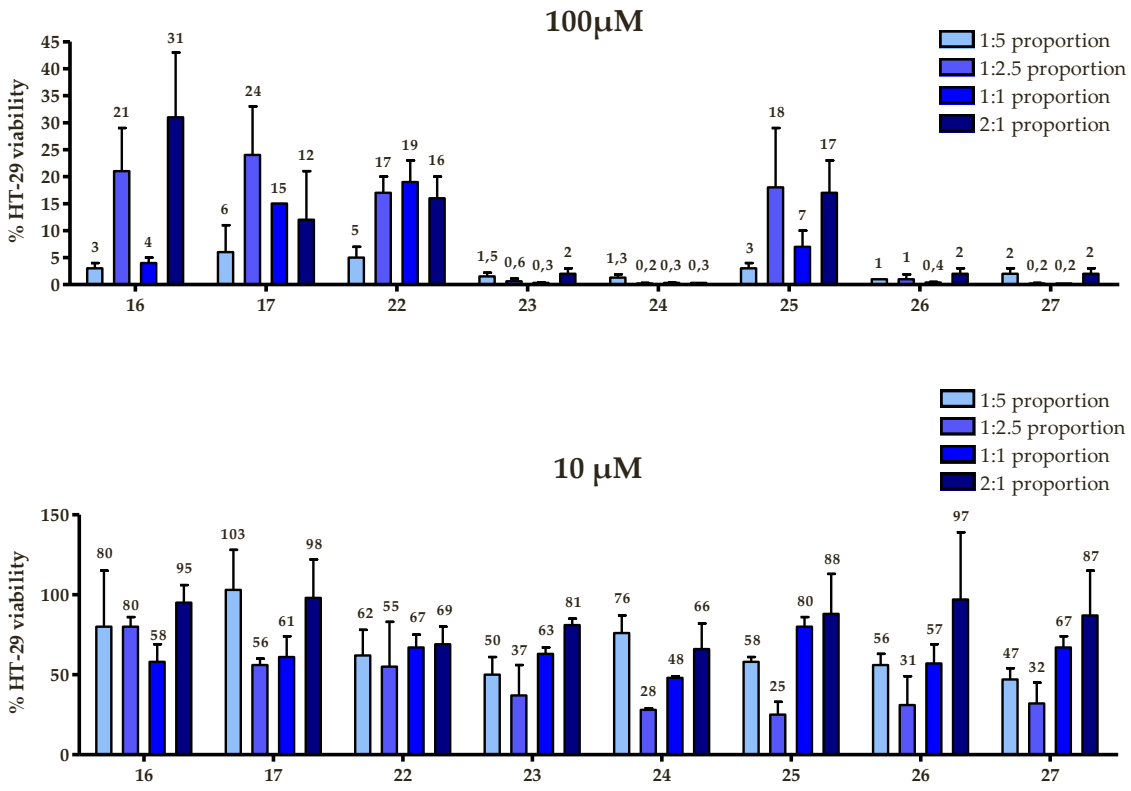

Fig. 5. HT-29 living cells (%) related to non-treated cells when co-cultured with different proportions of THP-1 at 100 and 10 μM doses.

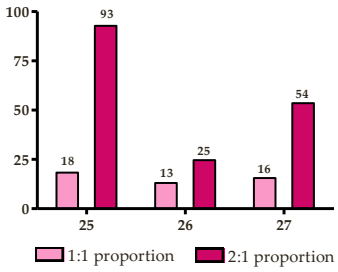

Fig. 6. IC_{50} values for chloro derivatives **25-27** in HT-29 co-cultured in different proportions of cancer and immune cells.

4. Discussion

We describe the synthesis and biological evaluation of twenty-seven derivatives bearing a tetrazole nucleus. First, we determined the effect on cancer cell viability in monocultures and co-cultures with THP-1 monocytes. We also investigated the activity of these compounds as PD-L1, CD-47, c-Myc and VEGFR-2 downregulators, together with their effect on PD-L1, CD-47 and VEGFR-2 distribution in cell membrane and on IL-6 and TNF-α secretion into the media. Tetrazoles **1** and **15**, together with nitrophenyl ones **2-14**, showed milder effects than the aminophenyl tetrazoles **16-27** on each biological target studied. In general, all compounds exhibited low antiproliferative activity on cancer cells, HT-29, A-549 and MCF-7 and on non-cancer cell line HEK-293. Compounds were more active against HT-29 cells, with *p*-methyl or *p*-halo benzyl derivatives **5**, **18**, **24** and **27** showing IC_{50} values in the micromolar range.

All these results suggests that the presence of an amine electron-donating group on the phenyl ring enhances and favors the antiproliferative activity of these derivatives. On the other hand, as regards substituents attached to benzylic system, compounds bearing chlorine, bromine and methyl groups were the ones exhibiting the best IC_{50} values against tumor cell lines. When these groups were occupying the relative 1,4 position in the benzylic system, the biological action was enhanced.

These structural features that enhance antiproliferative activity of the compounds, in general, also favor the other biological actions on PD-L1, CD-47, VEGFR and c-Myc in monocultures of cancer cells HT-29. Thus, at 100 μM doses we found that, again, aminophenyl derivatives were much more active than nitrophenyl ones, with bromo- and chlorobenzyl derivatives showing higher potencies (Tables 2.1 and 2.2). Our compounds showed a very mild effect on the targets except for total PD-L1 and c-Myc. Thus, chloro derivatives **25-27** showed around 50% inhibition rate on PD-L1 and for c-Myc compound **13** and chloro and bromo derivatives **22-27** showed inhibition rates around 30–45%, with *p*-bromo and *p*-chloro derivatives **24** and **27** being the most actives. We observed that the presence of a *meta*- or *para*- halogenated benzyl group attached to tetrazole ring is a relevant structural feature enhancing c-Myc inhibitory activity.

Besides, the effect on c-Myc and PD-L1 inhibition has been shown to be dose-dependent, in contrast to that observed for CD-47. For example, at 10 μM **25-27** derivatives CD-47 expression is inhibited by 25%, whereas at 100 μM the effect was negligible. This reveals the multi-targeted mode of action of the compounds we are presenting here.

Halogenated compounds **23**, **24**, **26** and **27** also inhibited cell proliferation by inducing apoptosis at 100 μM. This was confirmed by flow cytometry with an apoptotic cell population of around 65% and by observation of altered cell morphology (see Fig. 2). Again, *para*-halo substituted derivatives, together with the *meta* ones, showed the best results. These results on apoptosis induction correlate with the inhibition action on c-Myc (see Fig. 9) confirming the relationship between c-Myc inhibition and the pro-apoptotic effect [24].

The effect of the synthesized compounds on cell viability in co-cultures of HT-29 cells with immune THP-1 cells was assessed by flow cytometry and again the presence of amine electron-donating group in the phenyl unit dramatically increased the effect, going from 40% to 85% of cancer cells alive for derivatives with electron-withdrawing nitro group to 5–30% for some of the amine derivatives (see Fig. 3). Again, we

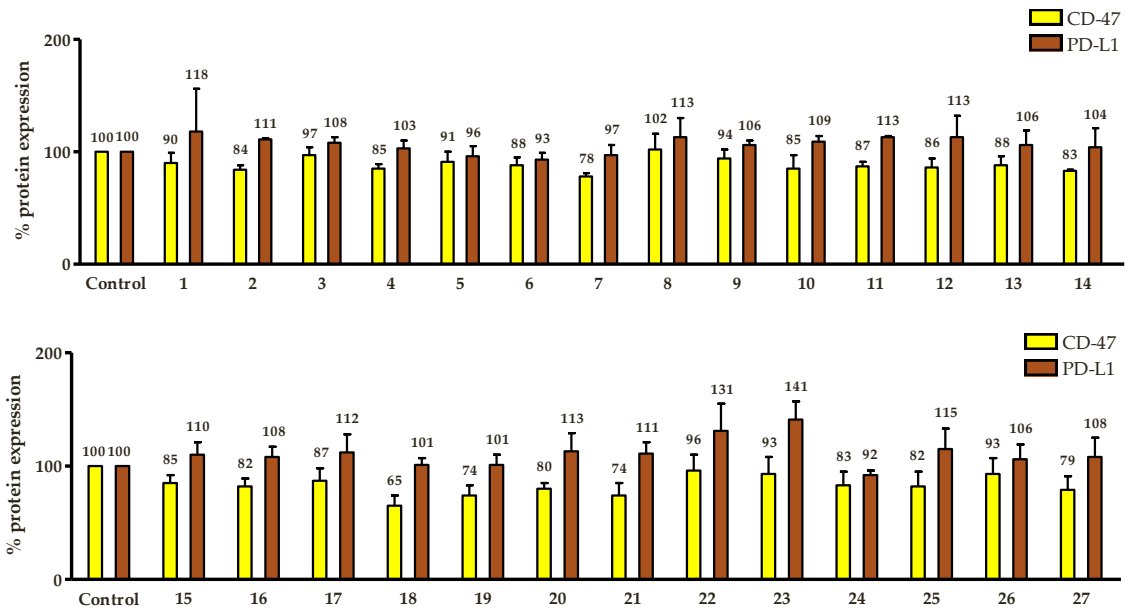

Fig. 7. Relative amount (%) of surface CD-47 and PD-L1 related to non-treated cells. Data are expressed as means ± SD for triplicates.

Table 4
Concentration of TNF-α in cell media from co-cultures HT-29/THP-1, at different proportions, after 48 h of treatment at 100 μM doses of compounds. Data are expressed as means ± SD for triplicates.

Compound	TNF-α (pg/mL) (1:5 proportion)	TNF-α (pg/mL) (2:1 proportion)
Control	58 ± 8	6.9 ± 0.2
22	328 ± 39	166 ± 46
23	70 ± 11	290 ± 64
24	149 ± 32	322 ± 9
25	266 ± 45	194 ± 22
26	163 ± 29	221 ± 8
27	74 ± 17	270 ± 59

found that the same structural features that enhanced the anti-proliferative activity of the compounds also favor the inhibition of cancer cell viability in co-cultures, highlighting among all the compounds haloderivatives **22-27**.

It is worth mentioning that our compounds did not affect the viability of THP-1 cells as it is shown in Fig. 4.

A further study carried out with the most active derivatives **16-17** and **22-27**, using different proportions of cancer cells and THP-1 monocytes, confirmed the potential as immunomodulators of *meta*- and *para*-bromo derivatives **23**, **24** and chlorotetrazoles **26** and **27**, since the proportion of cancer cells alive was always lower than 5% at doses of 100 μM and remained lower than 30% at 10 μM. The immunomodulation against cancer cells is clearly manifested by the fact that IC_{50} values for chloro derivatives **26** and **27** went from 100 μM in monoculture of HT-29 to about 15 μM in co-culture of HT-29 and THP-1. This means that the anti-proliferative effect on cancer cells is greatly improved in a more complex environment such as the one we have in the co-cultures with monocytic THP-1 cells. The mechanism of this improvement and enhancement of the anti-cancer effect observed in the presence of immune cells deserves further study, which is far from the objectives we had set for the present work. As far as now we have to say that chloro-derivatives **25-27** reduced living THP-1 cells to about 35–50% when monocultured at 100 μM doses. These values correlated with a 65–75% inhibition of the presence of PD-L1 on the surface of the monocytes compared to untreated cells. The effect is so high that it is still quite significant at 10 μM doses.

The fact that the compounds stimulate the production of TNF-α in co-cultures of cancer cells and THP-1 monocytes could be one of the reasons for the enhanced anti-cancer effect in these co-cultures compared to cancer cell monocultures. And also, the protective effect on monocytes, only in the co-culture environment, thus promoting the activation of immune cells against cancer cells. This is in line with the studies considering TNF-α as a mediator of anti-tumor immune responses [25] and those clinical studies that demonstrate that in some cancer immunotherapies, a co-administration with TNF-α antagonists have shown

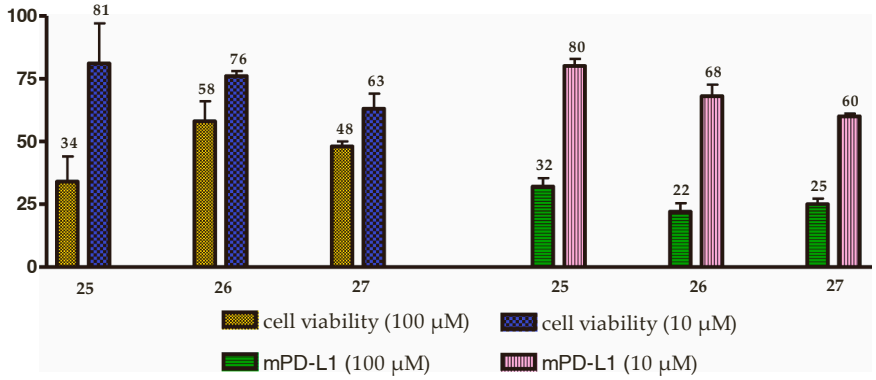

Fig. 8. Cell viability and expression of mPD-L1 for compounds **25**, **26** and **27** at 100 μM and 10 μM. Data are expressed as means ± SD for triplicates.

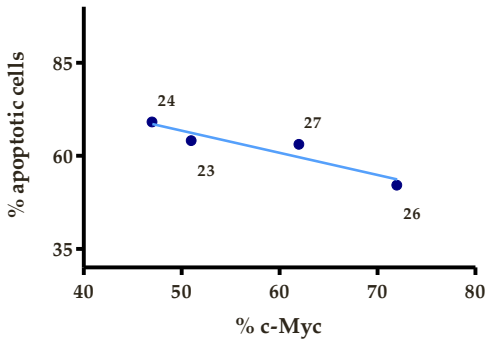

Fig. 9. Correlation c-Myc inhibition and apoptosis induction.

depleted anti-tumor efficacy [26]. All points out that a TNF-α release boosts an acute immune response against cancer cells.

5. Conclusion

In conclusion, we have developed a series of tetrazole-bearing small molecules with potent immunodulatory activity against cancer cell proliferation. The effect obtained with the halo derivatives, especially with chloro derivatives **26** and **27**, is remarkable as it improves with increasing complexity of the media, offering excellent candidates for oncoimmunological strategies and new, more effective, anti-cancer therapies.

Further experiments are needed to elucidate the mode of action of these compounds. We are also planning future in vivo assays to confirm anti-cancer activity of some of these compounds.

Funding Source

All sources of funding should be acknowledged, and you should declare any extra funding you have received for academic research of this work. If there are none state 'there are none'.

Funding

This work was supported by Grant PID2021–1267770B-100 funded by MCIN/AEI/ 10.13039/501100011033 and by "ERDF A way of making Europe" and by Universitat Jaume I (project UJI-B2021–46). A. P.-L. appreciates the FPI contract from Generalitat Valenciana (ACIF/ 2020/341).

Credit authorship contribution statement

Eva Falomir: conceptualization, data curation, funding acquisition, formal analysis, investigation, methodology, project administration, resources, software, supervision, validation, visualization, writing-original draft, writing-review & editing. **Miguel Carda**: conceptualization, data curation, funding acquisition, methodology, project administration, resources, supervision, writing-original draft, writing-review & editing. **Alberto Pla-López**: data curation, formal analysis, investigation, resources, software, validation, visualization, writing-original draft, writing-review & editing.

Declaration of Competing Interest

There are none.

Data Availability

Data will be made available on request.

Acknowledgements

Authors are grateful to SCIC of the Universitat Jaume I for providing NMR, mass spectrometry and flow cytometry facilities.

Appendix A. Supporting information

Supplementary data associated with this article can be found in the online version at doi:10.1016/j.biopha.2023.115668.

References

[1] N. El-Sayes, A. Vito, K. Mossman, Tumor heterogeneity: a great barrier in the age of cancer immunotherapy, Cancers 13 (*4*) (2021) 806, https://doi.org/10.3390/cancers13040806.
[2] R. Baghban, L. Roshangar, R. Jahanban-Esfahlan, K. Seidi, A. Ebrahimi-Kalan, M. Jaymand, S. Kolahian, T. Javaheri, P. Zare, Tumor microenvironment complexity and therapeutic implications at a glance, Cell Commun. Signal. 18 (2020) 1–19, https://doi.org/10.1186/s12964-020-0530-4.
[3] L. Pecorino. Molecular Biology of Cancer, 5th ed., Oxford University Press, 2021. ISBN: 9780198833024.
[4] T.L. Whiteside, The tumor microenvironment and its role in promoting tumor growth, Oncogene 27 (2008) 5904–5912, https://doi.org/10.1038/onc.2008.271.
[5] F. Emami, R. Duwa, A. Banstola, S.M. Woo, T.K. Kwon, S. Yook, Dual receptor specific nanoparticles targeting EGFR and PD-L1 for enhanced delivery of docetaxel in cancer therapy, Biomed. Pharm. 165 (2023) 115023–115037, https://doi.org/10.1016/j.biopha.2023.115023.
[6] C.V. Dang, MYC on the path to cancer, Cell 149 (2012) 22–35, https://doi.org/10.1016/j.cell.2012.03.003.
[7] J.N. Gnanaprakasam, R. Wang, C-Myc in regulating immunity: metabolism and beyond, Genes 8 (2017) 88–103, https://doi.org/10.3390/genes8030088.
[8] S.C. Casey, L. Tong, Y. Li, R. Do, S. Walz, K.N. Fitzgerald, A.M. Gouw, V. Baylot, I. Gutgemann, M. Eilers, et al., MYC regulates the anti-tumor immune response through CD47 and PD-L1, Science 352 (2016) 227–231, https://doi.org/10.1126/science.aac9935.
[9] H. Chen, H. Liu, G. Qing, Targeting oncogenic Myc as a strategy for cancer treatment, Sig. Transduct. Target Ther. 3 (2018) 5, https://doi.org/10.1038/s41392-018-0008-7.
[10] M. Binnewies, E.W. Roberts, K. Kersten, Understanding the tumor immune microenvironment (TIME) for effective therapy, Nat. Med 24 (2018) 541–550, https://doi.org/10.1038/s41591-018-0014.
[11] D. Riemann, W. Schütte, S. Turzer, B. Seliger, M. Möller, High PD-L1/CD274 expression of monocytes and blood dendritic cells is a risk factor in lung cancer patients undergoing treatment with PD1 inhibitor therapy, Cancers 12 (2020) 2966, https://doi.org/10.3390/cancers12102966.
[12] M. Nagano, K. Saito, Y. Kozuka, T. Mizuno, T. Ogawa, M. Katayama, PD-L1 expression on circulating monocytes in patients with breast cancer, Breast Cancer, Local. Adv. (2018) *29*, https://doi.org/10.1093/annonc/mdy427.008.
[13] L.V. Marchenko, A.D. Nikotina, N.D. Aksenov, J.V. Smagina, B.A. Margulis, I. V. Guzhova, Phenotypic characteristics of macrophages and tumor cells in coculture, Cell Tissue Biol. 60 (2018) 357–364, https://doi.org/10.1134/S1990519×18050036.
[14] A. Montfort, C. Colacios, T. Levade, N. Andriu-Abadie, N. Meyer, S. Ségui, The TNF paradox in cancer Progression and Immunotherapy, Front. Immunol. 10 (2019) 1818–1823, https://doi.org/10.3389/firmmu.2019.01818.
[15] R. Gil-Edo, S. Espejo, E. Falomir, M. Carda, Synthesis and biological evaluation of potential oncoimmunomodulator agents, Int. J. Mol. Sci. 24 (2023) 2614, https://doi.org/10.3390/ijms24032614.
[16] C. Martín-Beltrán, R. Gil-Edo, G. Hernández-Ribelles, R. Agut, P. Marí-Mezquita, M. Carda, E. Falomir, Aryl urea based scaffolds for multitarget drug discovery in anticancer immunotherapies, Pharmaceuticals 14 (2021) 337, https://doi.org/10.3390/ph14040337.
[17] L. Conesa-Milián, E. Falomir, J. Murga, M. Carda, J.A. Marco, Novel multitarget inhibitors with antiangiogenic and immunomodulator properties, Eur. J. Med. Chem. 148 (2019) 87–98, https://doi.org/10.1016/j.ejmech.2019.03.012.
[18] L. Conesa-Milián, E. Falomir, J. Murga, M. Carda, J.A. Marco, Synthesis and biological evaluation as antiangiogenic agents of ureas derived from 3′-aminocombretastatin A-4, Eur. J. Med. Chem. 162 (2019) 781–792, https://doi.org/10.1016/j.ejmech.2018.11.023.
[19] A. Pla-López, R. Castillo, R. Cejudo-Marín, O. García-Pedrero, M. Bakir-Laso, E. Falomir, M. Carda, Synthesis and bio-logical evaluation of small molecules as potential anticancer multitarget agents, Int. J. Mol. Sci. 23 (2022) 7049, https://doi.org/10.3390/ijms23137049.
[20] F. Lopes-Coelho, F. Martins, S.A. Pereira, J. Serpa, Anti-angiogenic therapy: current challenges and future perspectives, Int. J. Mol. Sci. 22 (7) (2021) 3765, https://doi.org/10.3390/ijms22073765.
[21] L. Skalniak, K.M. Zak, K. Guzik, K. Magiera, B. Musielak, M. Pachota, et al., Small-molecule inhibitors of PD-1/PD-L1 immune checkpoint alleviate the PD-L1-induced exhaustion of T-cells, Oncotarget 8 (2017) 72167–72181, https://doi.org/10.18632/oncotarget.20050.

[22] P. Patowary, B. Deka, D. Bharali, Tetrazole moiety as a pharmacophore in medicinal chemistry: a review, Malar. Contr. Élimin 10 (2021) 5–16, https://doi.org/10.37421/2470-6965.2021.10.167.
[23] A.K. Kabi, S. Sravani, S. Gujjarappa, A. Garg, N. Vodnala, U. Tyagi, D. Kaldhi, R. Velayutham, V. Singh, S. Gupta, C.C. Malakar, An overview on biological evaluation of tetrazole derivatives, Nanostruct. Biomater.: Basic Struct. Appl. (2022) 307–349, https://doi.org/10.1007/978-981-16-8399-2-8.
[24] S.K. Madden, A.D. de Araujo, M. Gerhardt, Taking the Myc out of cancer: toward therapeutic strategies to directly inhibit c-Myc, Mol. Cancer 20 (2021) 3–21, https://doi.org/10.1186/s12943-020-01291-6.
[25] D. Laha, R. Grant, P. Mishra, N. Nilubol, The role of tumor necrosis factor in manipulating the immunological response of tumor microenvironment, Front. Immunol. 12 (2021), 656908, https://doi.org/10.3389/fimmu.2021.656908.
[26] P. Berraondo, M.F. Sanmamed, M.C. Ochoa, Cytokines in clinical cancer immunotherapy, Br. J. Cancer 120 (2019) 6–15, https://doi.org/10.1038/s41416-018-0328-y.